X-ray absorption spectroscopy of GeO_2 glass to 64 GPa

2014 J. Phys.: Condens. Matter 26 035104

(http://iopscience.iop.org/0953-8984/26/3/035104)

IOP Publishing Journal of Physics: Condensed Matter

J. Phys.: Condens. Matter **26** (2014) 035104 (9pp) doi:10.1088/0953-8984/26/3/035104

X-ray absorption spectroscopy of GeO_2 glass to 64 GPa

Xinguo Hong[1,5], Matthew Newville[2], Thomas S Duffy[3,5], Stephen R Sutton[2,4] and Mark L Rivers[2,4]

[1] Mineral Physics Institute, Stony Brook University, Stony Brook, NY 11794, USA
[2] Center for Advanced Radiation Sources, University of Chicago, Chicago, IL 60637, USA
[3] Department of Geosciences, Princeton University, Princeton, NJ 08544, USA
[4] Department of Geophysical Sciences, University of Chicago, Chicago, IL 60637, USA

E-mail: xhong@bnl.gov, xinguo.hong@gmail.com and duffy@princeton.edu

Received 20 September 2013, in final form 29 October 2013
Published 28 November 2013

Abstract

The structural behavior of GeO_2 glass has been investigated up to 64 GPa using results from x-ray absorption spectroscopy in a diamond anvil cell combined with previously reported density measurements. The difference between the nearest Ge–O distances of glassy and rutile-type GeO_2 disappears at the Ge–O distance maximum at 20 GPa, indicating completion of the tetrahedral–octahedral transition in GeO_2 glass. The mean-square displacement σ^2 of the Ge–O distance in the first Ge–O shell increases progressively to a maximum at 10 GPa, followed by a substantial reduction at higher pressures. The octahedral glass is, as expected, less dense and has a higher compressibility than the corresponding crystalline phase, but the differences in Ge–O distance and density between the glass and the crystals are gradually eliminated over the 20–40 GPa pressure range. Above 40 GPa, GeO_2 forms a dense octahedral glass with a compressibility similar to that of the corresponding crystalline phase (α-PbO_2 type). The EXAFS and XANES spectra show evidence for subtle changes in the dense glass continuing to occur at these high pressures. The Ge–O bond distance shows little change between 45–64 GPa, and this may reflect a balance between bond shortening and a gradual coordination number increase with compression. The density of the glass is similar to that of the α–PbO_2-type phase, but the Ge–O distance is longer and is close to that in the higher-coordination pyrite-type phase which is stable above ~60 GPa. The density data provide evidence for a possible discontinuity and change in compressibility at 40–45 GPa, but there are no major changes in the corresponding EXAFS spectra. A pyrite-type local structural model for the glass can provide a reasonable fitting to the XAFS spectra at 64 GPa.

(Some figures may appear in colour only in the online journal)

1. Introduction

The high-pressure behavior of SiO_2 and GeO_2 has been extensively investigated because of their importance in condensed-matter physics, materials science, and geology. Germanium dioxide (GeO_2) is regarded as a chemical and structural analog of silica (SiO_2) [1], displaying similar compression behavior but at lower pressures. The well-known pressure response of these glasses is the evolution from corner-sharing tetrahedra at ambient conditions to a dense octahedrally coordinated glass at high pressure [2, 3]. GeO_2 glass is of particular interest because the local structure of Ge atoms can be studied at high pressures by x-ray absorption fine structure (XAFS) techniques in a diamond anvil cell (DAC). Despite previous investigations [2–12], detailed understanding of the short-range order (SRO) in the first coordination shell and intermediate-range order (IRO) in more distant shells of GeO_2 and SiO_2 glasses is still lacking. The nature of the transition to more highly coordinated structures is still a matter of debate [1, 2, 4, 6–15].

A first-order-like phase transition in GeO_2 glass was initially proposed based on the rapid change of the Ge–O

[5] Authors to whom any correspondence should be addressed.

distances observed over a narrow pressure range between 7 and 9 GPa [2]. However, no abrupt change in the Ge coordination was observed by recent experiments using neutron diffraction [4, 7, 10, 12], x-ray diffraction [4, 8], and XAFS [6, 9]. Neutron and x-ray diffraction studies [4, 10] suggest a continuous transition from predominantly four-fold to five-fold and finally to six-fold coordinated glass with pentahedral units dominating over the range ∼5–10 GPa. Moreover, theoretical simulations [5, 12, 13] also support a continuous transition mechanism with a mixture of four-fold, five-fold, and six-fold Ge, with fully six-fold Ge occurring above 30 GPa. A continuous formation of distorted square-pyramidal GeO_5 at 8 GPa was further proposed by simulations with quantitative agreement with neutron diffraction data [12]. A recent XAFS study [9] suggests that a transition region dominated by a mixture of four-fold and five-fold units encompasses the entire 6–30 GPa range, analogous to behavior observed for SiO_2 (10–25 GPa transition region) [16]. On the other hand, inelastic x-ray scattering data suggest that five-coordinated species are never more than a minority of the structural units as the glass transitions from being four-fold to being six-fold coordinated [11]. The pressure at which a fully six-coordinated state occurs is also unclear, with existing experiments suggesting values ranging from greater than 9 GPa to as high as 30 GPa [2, 4, 6, 8–10].

Crystalline GeO_2 exhibits a series of phase transitions under compression. The stable form of GeO_2 at ambient conditions is the six-coordinated rutile structure ($P4_2/mnm$). The quartz polymorph ($P3_221$) of GeO_2 is metastable but transforms to the rutile-type structure at ∼10 GPa [15]. The rutile phase undergoes a second-order ferroelastic transition to the $CaCl_2$-type ($Pnnm$) phase at 19–25 GPa [17, 18]. This transition occurs via compression of the weakest elongated axial Ge–O bonds of the rutile octahedron. At ∼30–36 GPa, the $CaCl_2$-type phase transforms to the α-PbO_2 phase ($Pbcn$) via a first-order mechanism with a small (1.1%) density change [19]. The $CaCl_2$ and α-PbO_2 phases also exhibit octahedral coordination. A further first-order transition to the pyrite-type structure ($Pa\bar{3}$) with 6 + 2 coordination (six oxygen ions at ∼1.8 Å and two additional O^{2-} at 2.6 Å) occurs at 59–66 GPa with a large volume change of nearly 6% [19]. No further transformations are expected until multi-megabar pressures are reached.

A number of theoretical studies of GeO_2 glass have been reported [5, 12, 13, 15, 20]. Molecular dynamics simulations of SiO_2 and GeO_2 glasses up to megabar pressures predict a certain degree of parallelism in the behavior of the glass and its crystalline counterparts with amorphous–amorphous transitions occurring over broad pressure intervals that correspond to the phase transition sequences in the solid [15]. Multiple amorphous–amorphous transitions and oxygen coordination greater than six above 40 GPa have been postulated in GeO_2 glass [15], similar to the case of SiO_2 glass at megabar pressures [21].

XAFS can be a powerful tool to determine the local (SRO) and higher-order (IRO) structure around absorber atoms [22] at high pressures. However, due to the Bragg reflections from the diamond anvils (so-called DAC imposed glitches), XAFS studies on GeO_2 glass at high pressure based on energy-dispersive (ED-XAFS) techniques [2, 9] are often limited to the near-edge (XANES) region or EXAFS with $k < 9$ Å^{-1}. While conventional energy-scanning XAFS (ES-XAFS) is highly accurate, it has long been regarded unsuitable for the DAC environment because of the significant absorption and diffraction effects of the diamond anvils [23].

Several methods have been proposed to eliminate DAC glitches for high-pressure XAFS measurements [24–27]. We have demonstrated an iterative method to obtain glitch-free XAFS data with the ES-XAFS method [24]. To understand the fundamental compression process of GeO_2 glass, we have used this technique to carry out *in situ* high-pressure XAFS measurements up to 64 GPa. The data quality and analysis techniques here are improved over the preliminary data presented earlier [24].

2. Experiment

GeO_2 glass samples were made by quenching GeO_2 melt at 1600 °C (donated by L Huang at Rensselaer Polytechnic Institute, New York). XAFS experiments were carried out on the Ge K-edge of the glass in transmission mode at the GeoSoilEnviroCARS bending magnet beamline 13-BM-D, advanced photon source (APS), Argonne National Laboratory. XAFS spectra were collected from 10 953 to 11 747 eV with 5 eV steps before the main edge, 0.5 eV steps from −10 to 25 eV across the main edge (11 110 eV), and 0.05 Å^{-1} steps in k-space to 13 Å^{-1} above the main edge. Seven scans were collected at different DAC orientations with a 1° step within an angle range of ±3° around the ω axis (vertical axis of the diffractometer). Princeton-manufactured standard and large-opening symmetrical DACs with 300 μm culet size and 2.1 mm thickness anvils were employed. The x-ray beam size was focused down to 15 μm using Kirkpatrick–Baez mirrors. Other experimental details can be found elsewhere [14].

To remove the glitches in the raw absorption spectra due to diamond Bragg reflections, an iterative method which was designed to progressively identify and eliminate DAC glitches was employed. Here, we provide a short summary of the basic method; a full description can be found elsewhere [24]. Initially, all the XAFS spectra from different ω orientations are averaged together. Next, each individual spectrum is compared to the average, and misfit criteria are applied to identify and remove glitches. Initially, the misfit criteria are relatively coarse, for example, deviations of 10%, 20%, and 5% in the pre-edge, edge, and post-edge regions, respectively, would trigger glitch removal from an individual spectrum. After this initial iteration, all the spectra are averaged together again, and the process is repeated with a successively more stringent misfit criterion applied each time to remove weaker glitches. Finally, when there is no change in the resultant averaged spectrum and all the glitch-removed spectra at each orientation are consistent with each other, the iterative process is completed. It typically takes several cycles to effectively remove all the diamond anvil imposed glitches. As a typical

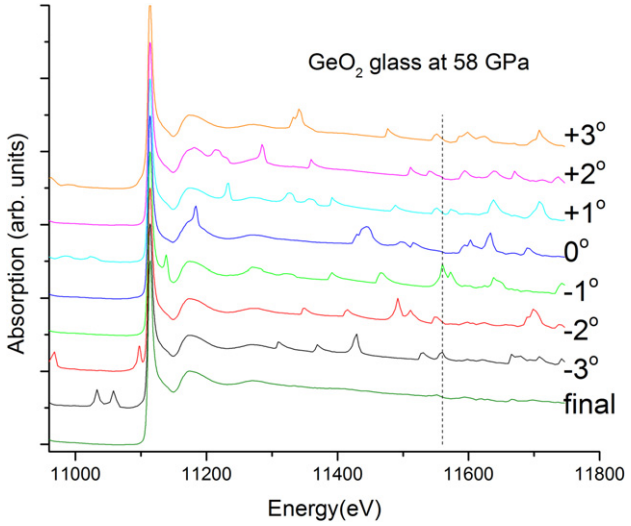

Figure 1. Ge K-edge XAFS of GeO_2 glass at 58 GPa obtained by classic energy-scan transmission mode across the diamond anvils at different ω angle settings. The x-ray absorption spectra show extra peaks due to Bragg diffraction by the single-crystal diamond anvils. The bottom curve shows the spectrum obtained after application of the glitch-removal algorithm. The vertical dashed line (11 560 eV) shows the extent of the energy range used in the analysis.

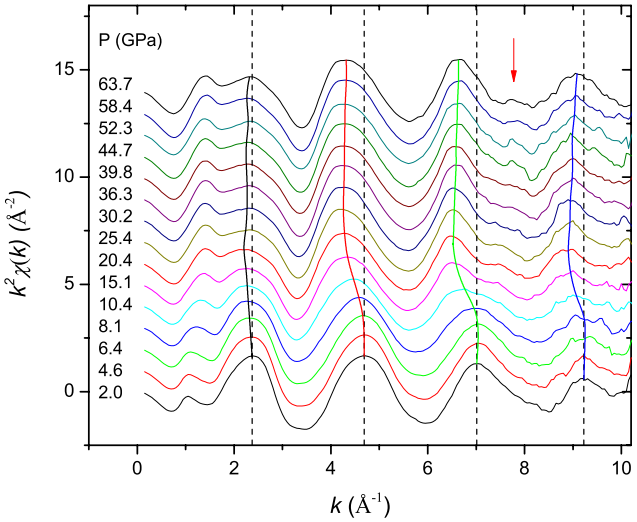

Figure 2. k^2-weighted XAFS spectra, $k^2\chi(k)$, for GeO_2 glass at high pressures. Dashed lines denote the four peak positions of the XAFS oscillations for tetrahedral GeO_2 glass at 2 GPa. Solid vertical curves are the corresponding peak positions determined by Gaussian fits at high pressures (listed at the left-hand side). The red arrow highlights the change in the XAFS oscillation profile (7–8 $Å^{-1}$) above 45 GPa.

example, after three iterations, the standard deviation of seven independent spectra to the average one is about 0.11% over the whole spectrum [24]. The method provides high-quality, glitch-free XAFS spectra above the Ge K absorption edge by 410 eV ($k = 10.4$ $Å^{-1}$). Further XAFS data processing and analysis were then performed with the ATHENA and ARTEMIS programs [28] of the IFEFFIT package [29].

3. Results and discussion

Figure 1 shows the typical multiple datasets of transmission Ge K-edge XAFS for GeO_2 glass at 58 GPa with the diamond anvil cell at different ω angle settings of 0°, ±1°, ±2°, and ±3° with respect to the incident beam. All these spectra were overlapped and aligned using the iterative algorithm [24] for the elimination of glitches. The bottom curve shows the spectrum obtained after application of the glitch-removal algorithm. Each composite point is typically based on at least three independent XAFS scans. The upstream vertical focusing mirror at sector 13-BM-D of the APS is coated with a platinum layer (11 564 eV, L_3-edge energy of platinum). To allow reliable data extraction of the x-ray absorption coefficient, the extent of the energy range is therefore limited to below 11 560 eV (figure 1, dashed line) to avoid the absorption edge of Pt. Figure 2 shows the k^2-weighted $\chi(k)$ XAFS spectra obtained for GeO_2 glass at high pressures. Solid lines mark the four peak positions of the XAFS oscillations, which were determined by Gaussian fits, while dashed lines are the peak positions for tetrahedral GeO_2 glass at 2 GPa. It can be seen that all four peaks shift to lower k values with the respective minima near 20 GPa. There is another prominent pressure-induced change in XAFS amplitudes and frequencies (6–8 $Å^{-1}$) at 6–20 GPa. The

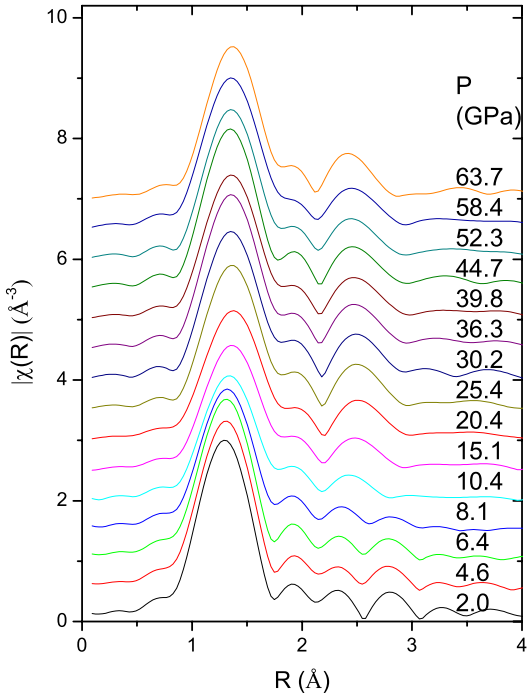

Figure 3. XAFS Fourier transform moduli, $|\chi(R)|$, for GeO_2 glass at high pressures. Note the merging of two peaks (2.2–3 Å) at 10.4 GPa.

XAFS spectra at low pressures (≤6.4 GPa) are very similar, as are those at >20 GPa, which indicates that the major change in the Ge local environment occurs over the 6–20 GPa range. It should be noted that there is a minor change in the XAFS oscillation profile (7–8 $Å^{-1}$) above 45 GPa, while the fourth peak (9 $Å^{-1}$) shifts to high k values.

Figure 3 shows the XAFS amplitude, $|\chi(R)|$, from the Fourier transform of $k^2\chi(k)$ for the measured EXAFS spectra

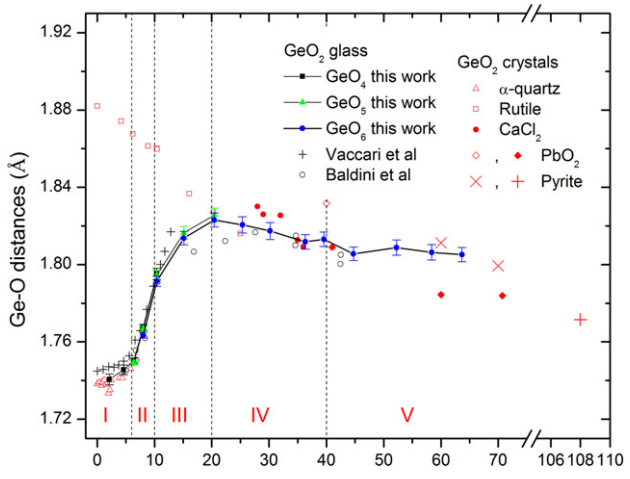

Figure 4. Evolution of the nearest Ge–O distance as a function of pressure using tetrahedral (■), pentahedral (▲) and octahedral (●) coordinated models. The error bar shows one standard deviation uncertainty. Ge–O distances from previous XAFS experiments [6, 9], as well as crystalline α-quartz (Δ [32, 36]), rutile (□ [17]), $CaCl_2$ (● [17]), PbO_2-type (◊ [19]; ♦ [33, 34]) and pyrite-type (× [19]; + [33]) samples are shown for comparison.

(figure 2). A Hanning window was applied in the k range 2–10.1 $Å^{-1}$ without impairing the observed change in XAFS oscillations (6–8 $Å^{-1}$). As the pressure increases, the main peak, which corresponds to the first Ge–O distance, clearly elongates at 6–15 GPa (from 1.75 to 1.81 Å, figure 4). The two peaks of the XAFS moduli $|\chi(R)|$ in the range 2.2–3.0 Å (without phase correction) merge together above 10.4 GPa, reflecting significant pressure-induced modification at IRO distances.

Determination of the coordination number and its variance for a given atom requires accurate measurement of the EXAFS amplitude [30]. Changes in sample thickness do not affect the interatomic Ge–O distance but have significant influence on the EXAFS amplitude [30]. For DAC samples, the thickness cannot be controlled at each pressure step, and the sample becomes thinner with increasing pressure [31]. Due to these uncertainties, the Ge–O distance obtained from EXAFS analysis is the most reliable parameter to characterize the pressure response of GeO_2 glass.

The data were analyzed using structural models for the Ge–O first shell consisting of tetrahedral, pentahedral, and octahedral units. Figure 4 shows the resulting evolution of the nearest Ge–O distance from the first-shell analysis for these cases. There is good agreement in the transition region from 6 to 15 GPa for all of the models employed. The XAFS parameters, amplitude and E_0, were determined by free fitting at first for tetrahedral (≤6.4 GPa) and octahedral (20–64 GPa) models, respectively, and then fixed for the respective tetrahedral or octahedral region covering the transition range 6–15 GPa. The Ge–O distances obtained agree well with the values reported by Vaccari *et al* [6] and Baldini *et al* [9] below 10 GPa, and the values reported by Baldini *et al* [9] at 28–44 GPa. In the intermediate pressure range, our results show that the Ge–O distance reaches a peak at about 20 GPa and declines slowly thereafter. In contrast, the results of Baldini *et al* [9] show a smaller Ge–O distance at 20 GPa, which continues to rise until about 30 GPa. The divergence between the two studies at 15–25 GPa may be due to either the narrow data range (<8 $Å^{-1}$) or DAC glitches not fully corrected in the previous work [9]. For comparison, the Ge–O distances of the corresponding crystalline GeO_2 structures of α-quartz [32], rutile [17], $CaCl_2$ [17], α-PbO_2 [19, 33, 34], and pyrite [19, 33] types are shown in figure 4. These were calculated from reported structural parameters from theory or experiment using the software ATOMS [35].

The variation of the Ge–O bond distance can give important insights into the high-pressure behavior of the glass as it reflects the competing processes of shortening due to compression and lengthening due to increases in coordination number. At low pressures (<6 GPa), the Ge–O distance appears consistent with those of four-coordinated α-quartz GeO_2 determined by neutron diffraction [32] and XAFS [36]. Up to 6 GPa, the Ge–O distances increase only slightly, showing similar pressure dependence to α-quartz GeO_2. This indicates that the glass remains tetrahedral in structure and that there is little encroachment of more distant O atoms into the first Ge–O tetrahedral shell [4]. Above 6 GPa, there is a rapid increase in Ge–O distance at 6–10 GPa, followed by a shallower rise until a maximum is reached at 20 GPa. The increase at 6–10 GPa was first observed by Itie *et al* [2] and interpreted as evidence of a first-order transition to six-fold coordination such as occurs in rutile-type GeO_2. However, even at 10 GPa, the Ge–O distance is still far below the value in crystalline rutile GeO_2 at the corresponding pressure (figure 4). The convergence of Ge–O distances in glass and rutile-type GeO_2 by 20 GPa (figure 4) indicates that the tetrahedral–octahedral transition is not likely complete until this pressure. At 20–45 GPa, the Ge–O distance shows a shallow decrease similar to or shallower than the compression behavior of $CaCl_2$-type GeO_2 [17], and then remains nearly constant from 45 to 64 GPa. This suggests that the glass behavior at 20–45 GPa is dominated by compression of a mostly octahedral glass, while above 45 GPa the effects of a further coordination number increase (greater than six) may be counteracting the compression effect, resulting in a more constant Ge–O bond length.

The Debye–Waller (DW) factor, σ^2, which represents the mean-square displacement (disorder) in the Ge–O bond length, is expected to show significant variation during the collapse of tetrahedral units at high pressure [6, 9]. The DW factor, however, depends on measurement of accurate XAFS amplitude and is sensitive to the model employed in EXAFS fitting. The value of E_0 is slightly correlated to the Ge–O distance. To get an overall DW profile as a function of pressure, it is necessary to mitigate the correlation between the EXAFS amplitude and the DW factor. The parameters of XAFS amplitude and E_0 were set free in the first initial fitting using tetrahedral and octahedral models, respectively. The amplitude and E_0 obtained were then averaged over the entire pressure range and fixed in the subsequent XAFS modeling so as to minimize the correlation between the EXAFS amplitude and the DW factor, and between E_0 and the Ge–O distance. Figure 5 shows the pressure evolution of DW

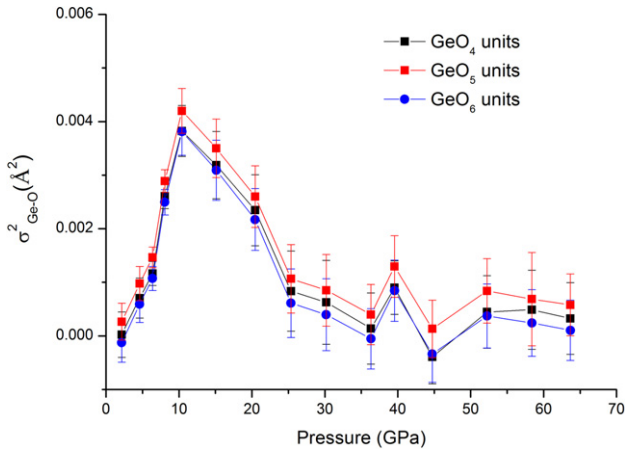

Figure 5. The pressure evolution of the Debye–Waller (DW) factor, σ^2, which was obtained from EXAFS analysis using GeO_4, GeO_5 and GeO_6 polyhedral units. For details, see the text.

factor, σ^2, obtained from EXAFS analysis using GeO_4, GeO_5, and GeO_6 polyhedral units. We can see a consistent behavior of the DW factor without any strong model dependence for the first Ge–O distance. As the pressure increases, the σ^2 value also increases and reaches a maximum at 10 GPa. It then progressively decreases to nearly a constant value above 25 GPa. This maximum in the DW factor indicates that the highest disorder in the first Ge–O shell occurs at 10 GPa. This may imply different structural units, including the possibility of pentahedral coordination GeO_5 units in the glass, as suggested by other studies [4, 5, 10, 12]. The termination of the σ^2 reduction near 25 GPa may be consistent with completion of the formation of octahedral GeO_6 units in GeO_2 glass, as supported by the Ge–O distances (figure 4). The difference in the DW factor between this work and a previous XAFS study [9] may come from the smaller k range in previous study with $k_{max} \sim 8 Å^{-1}$ using energy-dispersive (ED-XAFS) techniques.

To examine the behavior of octahedral GeO_2 glass up to 64 GPa, it is useful to compare the XANES and EXAFS spectra above 20 GPa. Figure 6(a) shows the Ge K-edge XANES spectra of GeO_2 glass at pressures of 20, 30, and 63.7 GPa, while figure 6(b) contains the difference spectra relative to the spectrum at 20 GPa. The XANES spectra of 20 and 30 GPa look quite similar. For the spectrum of 63.7 GPa, a strong peak appears at $E = 11\,116$ eV, and there is a large change in oscillation (figure 6(b)). This provides possible evidence for further modifications in GeO_2 glass above 30 GPa.

Figure 7(a) shows the k^2-weighted XAFS spectra $k^2\chi(k)$ for GeO_2 glass at pressures of 20.4, 30.2, and 63.7 GPa. The arrow highlights the changes in XAFS amplitudes and oscillations. The oscillation at 6–8 $Å^{-1}$ becomes more symmetric at higher pressures. Figure 7(b) shows the corresponding XAFS Fourier transform $|\chi(R)|$ and reveals that there are two changes in the octahedral glass. We can see that the peak of the nearest Ge–O distance is enhanced with a relatively narrow distribution above 30 GPa, which is consistent with the change in the DW factor (figure 5).

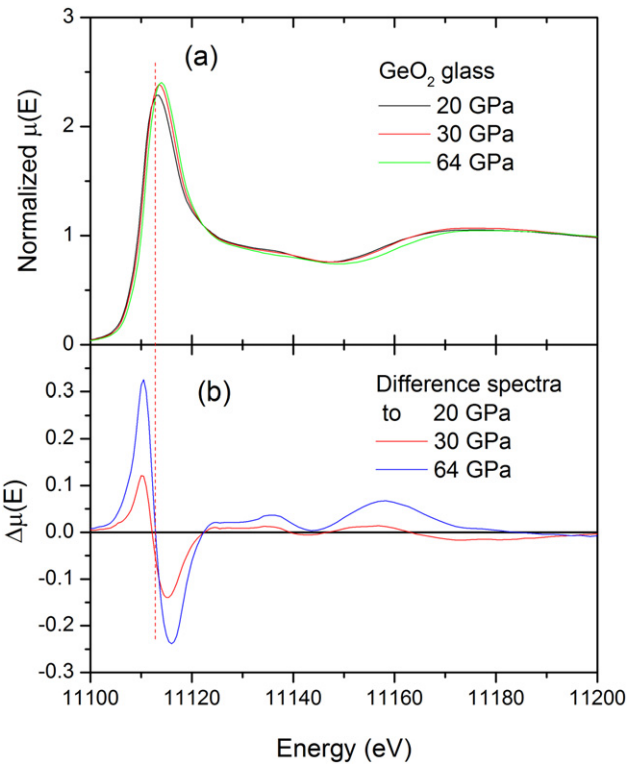

Figure 6. (a) Ge K-edge XANES spectra of GeO_2 glass at pressures of 20.4, 30.2 and 63.7 GPa; (b) the difference spectra compared to 20.4 GPa.

The other feature is the reduction of coordination distances at the second peak position (2.2–3 Å) as the pressure increases from 30 to 63.7 GPa. These observations illustrate that pressure-induced changes in GeO_2 glass do not terminate upon the completion of the tetrahedral–octahedral transition but subtle variations continue beyond this transition. In addition, the similarity of Ge–O distance (figure 4) between GeO_2 glass and the crystalline counterparts of rutile, $CaCl_2$, and pyrite is also notable.

Density is another key physical quantity for studying non-crystalline materials. An *in situ* density measurement technique was developed for samples contained in diamond anvil cells using x-ray absorption and simultaneous x-ray diffraction measurements [31]. The density of GeO_2 glass was determined up to 56 GPa [14, 31]. The maximum measured density was 7.56 g cm^{-3}, corresponding to more than a two-fold compression of the glass relative to its ambient pressure value. Figure 8 shows a comparison of all the density data for GeO_2 glass and crystals. For the crystalline phases, the symbols show experimental measurements whereas the colored solid lines show theoretical calculations using density functional theory. Below 6 GPa, the density increases strongly with pressure, likely reflecting the reduction of the cage size in the tetrahedral glass [14]. Above ~15 GPa, the rate of density increase is lowered. The reduction of Ge–O distance in this range (figure 4) reflects the compression effect on the local structure, and the gradual free-volume exhaustion of the network cage as the density gap between glassy and $CaCl_2$-type GeO_2 nearly closes by 35 GPa (figure 8). The

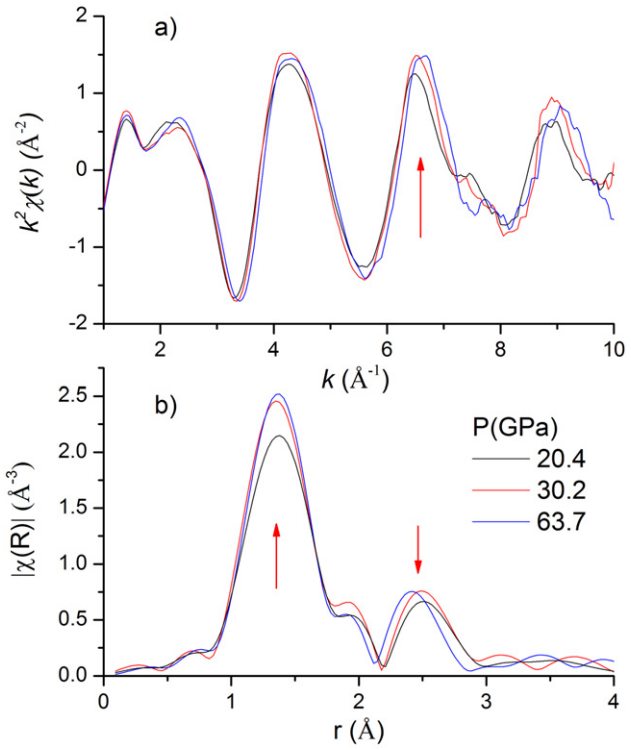

Figure 7. (a) XAFS $k^2\chi(k)$ for GeO_2 glass at pressures of 20.4, 30.2 and 63.7 GPa; (b) XAFS Fourier transform $|\chi(R)|$ for GeO_2 glass at 20.4, 30.2 and 63.7 GPa.

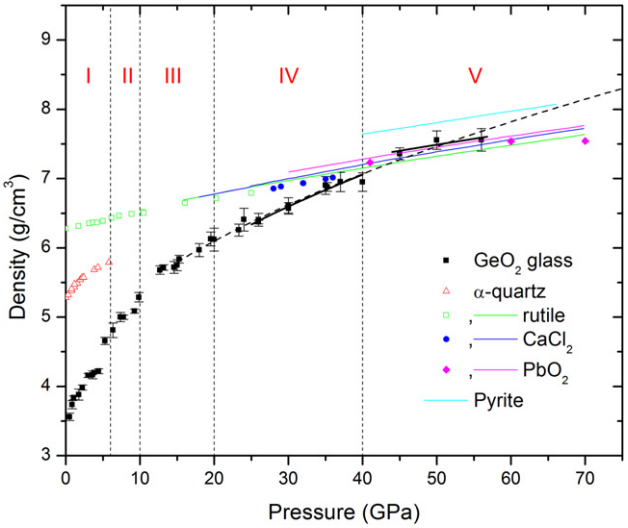

Figure 8. Density of GeO_2 glass at high pressure. For details, refer to [14, 31]. Densities of GeO_2 crystal phases from experiments are presented for comparison (as symbols): α-quartz (red Δ [32, 36]); rutile (green □) and $CaCl_2$ (blue ◯) from [17]; and PbO_2-type (magenta ♦) from [33, 34]. Solid lines show calculations of pressure–density relations for GeO_2 polymorphs: rutile (green), $CaCl_2$ (blue), PbO_2 (magenta) and pyrite (cyan) [19]. Solid black lines are the fits in the pressure ranges 25–40 GPa and 45–56 GPa to the third-order Birch–Murnaghan equation of state. The dashed black line shows a single fit to the Birch–Murnaghan equation over the 15–56 GPa pressure range.

octahedral GeO_2 glass in this pressure region would be a lower density and more compressible octahedral form in comparison with the rutile-type and $CaCl_2$-type GeO_2. These are typical behaviors for glass compared with their crystal counterparts.

The $CaCl_2$–PbO_2 phase transition (∼36 GPa) occurs via a first-order mechanism, but the density change is small (1.1%) [19]. At 35–40 GPa, the density of GeO_2 glass lies below that of α-PbO_2-type GeO_2 from theory [19] and experiment [33]. Between 40 and 45 GPa, there is a discontinuity (∼6%) in the density data, and the measured glass densities overlap those of the α-PbO_2 phase above 45 GPa (figure 8). The Ge–O bond distances remain almost constant above this pressure (figure 4). The data between 15 and 56 GPa were fit to a third-order Birch–Murnaghan equation (dashed black line, figure 8) yielding the parameters $\rho_0 = 4.5 \pm 0.08$ g cm^{-3}, $K_0 = 35.8 \pm 3.0$ GPa, and K_0' fixed at 4. Figure 8 also shows fits using two separate third-order equations of state for the data above and below 45 GPa.

Although only a few data points are available, the compression of GeO_2 glass above 45 GPa appears very similar to that for the crystalline forms of $CaCl_2$ type and PbO_2 type. This is in contrast to the data below 45 GPa, which clearly shows a higher compressibility for the GeO_2 glass. While a single third-order Birch–Murnaghan for the entire data set above 15 GPa can fit all the data within uncertainty, the compressibility of the glass predicted from the fit is much higher than that exhibited by the crystalline data above 45 GPa. Furthermore, a modest extrapolation of the data to 70 GPa shows that the predicted densities for GeO_2 glass start to exceed even those of the pyrite-type structure. Thus, a single continuous fit does not provide a satisfying explanation for the data. Using a fourth-order Birch–Murnaghan equation or a Vinet equation does not change this. The fit using separate equations of state above and below 40 GPa appears to overall provide a better description of the data. Given the uncertainties in the measurements, a volume discontinuity at 40–45 GPa cannot be unambiguously identified based on the present data. Furthermore, there is no strong change in the XAFS spectra in this pressure range. Further density and XAFS measurements are needed to clarify the behavior in this range.

A theoretical molecular dynamics study has predicted that GeO_2 glass may undergo transformations that parallel the corresponding crystalline transitions but over broader pressure ranges [15]. In particular, the simulations showed increases in coordination of the glass over pressure ranges that overlap the transition pressures for $CaCl_2$-α-PbO_2 and α-PbO_2-pyrite-type. In our study, both the density and compression behaviors of the glass are similar to those of the corresponding crystalline counterparts above 40 GPa, and the Ge–O bond distance shows less reduction with pressure than it does at lower pressures. Thus, clear changes in the behavior of the glass are observed in the same pressure range (40–60 GPa) where the smooth structural transition is predicted from the molecular dynamics data [15]. At 45 GPa and above, the measured densities of the glass overlap those of the α-PbO_2 phase, suggesting that the density difference between the glass

and crystalline counterparts becomes very small above this pressure.

In the crystalline counterpart, the first-order PbO_2-type to pyrite-type transition occurs at ~66 GPa with a large volume change of nearly 6.1% [19] (figure 8). At ~60 GPa, the Ge–O distance of GeO_2 glass is similar to that found for pyrite-type GeO_2 from theoretical calculations [19] (figure 4). The α-PbO_2-type structure has three separate Ge–O bond lengths exhibiting about 4–5% total variation. The average value at 71 GPa is 1.784 Å [34], lower than our observed values for the pyrite-type phase or the glass. The six O ions of the GeO_6 octahedron in the pyrite structure have the same distance from Ge, which agrees with the observed symmetrical $|\chi(R)|$ peak (figure 7(b)) and small DW factor σ^2 at 63.7 GPa (figure 5). In addition, EXAFS modeling (1–3 Å) based on a pyrite local structure for GeO_2 glass gives a good fitting for the XAFS spectra at 63.7 GPa with a goodness-of-fit parameter, R_w, of 0.006 and reduced chi-square value, down to 74.39. To keep the integrality of the pyrite structure, no change in the path degeneracies and relative amplitude, and the same distance variables were used for each coordination shell.

Figure 9 shows a comparison between the experimental spectrum and the theoretical calculations based on the Ge–O and Ge–Ge cluster of the pyrite-type in *R*-space (figure 9(a)) and back-transformed $|\chi(R)|$ (1–3 Å) in *q*-space (figure 9(b)). Beyond the nearest Ge–O distance (1.8 Å), there are two other Ge–O paths found at 2.41 Å. The structures of α-quartz, rutile, and $CaCl_2$-type GeO_2 have no additional Ge–O bond at 2–3 Å as the second Ge–O coordination shell, but PbO_2 and pyrite structures have such a Ge–O bond, at 2.8 Å and 2.6 Å, respectively. This result suggests that GeO_2 glass at 60 GPa bears some similarities to the pyrite-type structure, and this phase could be a useful analog of the glass at high pressure. The density of the glass, however, is closer to that of the α-PbO_2-type phase and less than that of the pyrite phase (figure 8).

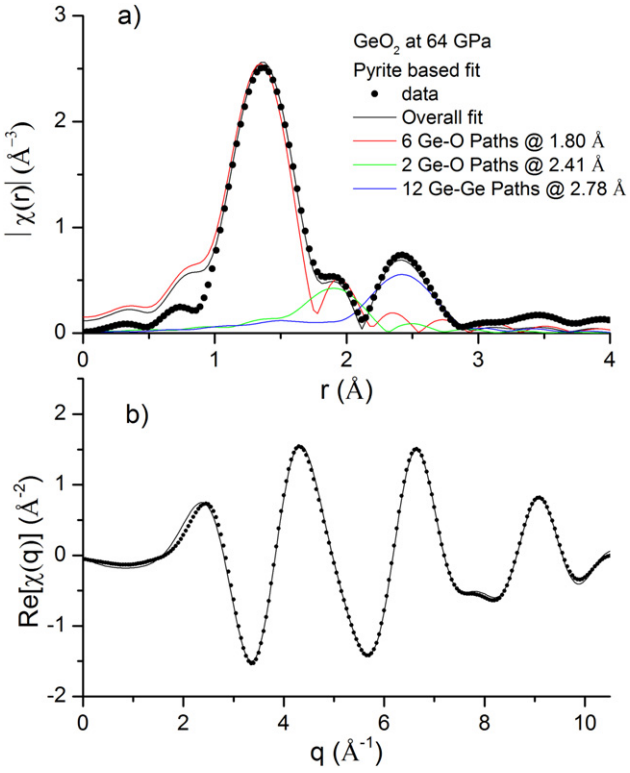

Figure 9. (a) Fourier transformation modulus, $|\chi(R)|$, of $k^2\chi(k)$ for GeO_2 glass at 63.7 GPa (full circles). The pyrite-based structural modeling (black line) yields 6 symmetric Ge–O paths at 1.80 Å (red line), 2 Ge–O paths at 2.41 Å (green line) and 12 Ge–O paths at 2.78 Å (blue line). (b) Comparison of back-transformed $|\chi(R)|$ at 1–3 Å between experimental data (full circles) and best-fit calculation (black line) in *q*-space.

4. Summary

New XAFS measurements combined with previous density data show that GeO_2 glass undergoes a continual structural evolution at high pressures. The high-pressure behavior of GeO_2 glass, when taken together with evidence for the formation of pentahedral GeO_5 units from other studies, can be divided into five distinct regions: (I) tetrahedral glass with GeO_4 units (<6 GPa); (II) formation of pentahedral GeO_5 units (~6–10 GPa); (III) formation of octahedral glass (~10–20 GPa); (IV) compressible octahedral glass with lower density than crystal counterparts (~20–40 GPa); (V) a dense octahedral glass (>40 GPa) with similar density and compressibility to the corresponding crystalline phases. Our results are generally consistent with those of a previous XAFS study [9], although our pressure ranges for different compression regimes are somewhat different, most notably in that we observe completion of the formation of octahedral glass near 20 GPa, instead of ~30 GPa as in the previous work.

At low pressures (<6 GPa), the Ge–O distance is consistent with that of α-quartz GeO_2, and the density increases strongly with pressure. At 6–20 GPa, significant changes in the XAFS spectra are observed. There is a rapid increase in Ge–O distance to 15 GPa, followed by a shallower rise to a maximum at 20 GPa. The density continues to increase strongly to 20 GPa. The Debye–Waller factor also increases, reaching a maximum value at 10 GPa, and declines to a minimum value above ~20 GPa. These observations are consistent with completion of the tetrahedral–octahedral transition at about 20 GPa. It should be noted that the tetrahedral–octahedral completion pressure roughly coincides with the values from *ab initio* calculations (19 GPa) [19], and experiments (25 GPa) [17] for the rutile-$CaCl_2$ phase transition in GeO_2.

The pressure range between 20 and 40 GPa is characterized by a continuous decrease in the Ge–O bond distance and an increase in density with a compressibility markedly greater than that of the crystalline phases of GeO_2. The differences in Ge–O bond length and density of the glass and the corresponding crystals slowly decreases and is eliminated by about 35–40 GPa. This region thus corresponds to a low-density, compressible, mostly octahedral glass. The completion pressure of the Ge–O distance shortening (35–40 GPa) corresponds roughly to

the crystalline $CaCl_2$-α-PbO_2-type (*Pbcn*) phase transition pressure (36 GPa) [19].

The XANES and XAFS spectra continue to show subtle changes above 30 GPa, suggesting further modifications of the glass structure at high pressures. A possible discontinuity in the density data is observed at 40–45 GPa, and there is a reduced compressibility of the glass above this pressure. However, there is no major change in the corresponding XAFS spectra, and the Ge–O bond distance remains nearly constant above 40 GPa. In this range, the density and compressibility of the glass become very similar to those of the corresponding crystalline phases. The Ge–O bond distance may reflect a balance between bond shortening under compression and bond lengthening due to a gradual coordination number increase. EXAFS modeling shows that the structure of the glass at the highest pressures can be successfully fit using a pyrite-type structure model as an analog for the glass.

Acknowledgments

We would like to thank D Weidner, X M Yu, L P Huang, S Dorfman, and S Lin for discussions and assistance. This research was supported by COMPRES under NSF EAR 11-57758. The GSECARS sector of APS is supported by the NSF (EAR-1128799) and the DOE (DE-FG02-94ER14466).

References

[1] Micoulaut M, Cormier L and Henderson G S 2006 The structure of amorphous, crystalline and liquid GeO_2 *J. Phys.: Condens. Matter* **18** R753

[2] Itie J P, Polian A, Calas G, Petiau J, Fontaine A and Tolentino H 1989 Pressure-induced coordination changes in crystalline and vitreous GeO_2 *Phys. Rev. Lett.* **63** 398–401

[3] Durben D J and Wolf G H 1991 Raman spectroscopic study of the pressure-induced coordination change in GeO_2 glass *Phys. Rev.* B **43** 2355–63

[4] Guthrie M, Tulk C A, Benmore C J, Xu J, Yarger J L, Klug D D, Tse J S, Mao H k and Hemley R J 2004 Formation and structure of a dense octahedral glass *Phys. Rev. Lett.* **93** 115502

[5] Shanavas K V, Garg N and Sharma S M 2006 Classical molecular dynamics simulations of behavior of GeO_2 under high pressures and at high temperatures *Phys. Rev.* B **73** 094120

[6] Vaccari M, Aquilanti G, Pascarelli S and Mathon O 2009 A new EXAFS investigation of local structural changes in amorphous and crystalline GeO_2 at high pressure *J. Phys.: Condens. Matter* **21** 145403

[7] Drewitt J W E, Salmon P S, Barnes A C, Klotz S, Fischer H E and Crichton W A 2010 Structure of GeO_2 glass at pressures up to 8.6 GPa *Phys. Rev.* B **81** 014202

[8] Mei Q, Sinogeikin S, Shen G, Amin S, Benmore C J and Ding K 2010 High-pressure x-ray diffraction measurements on vitreous GeO_2 under hydrostatic conditions *Phys. Rev.* B **81** 174113

[9] Baldini M, Aquilanti G, Mao H k, Yang W, Shen G, Pascarelli S and Mao W L 2010 High-pressure EXAFS study of vitreous GeO_2 up to 44 GPa *Phys. Rev.* B **81** 024201

[10] Salmon P S, Drewitt J W E, Whittaker D A J, Zeidler A, Wezka K, Bull C L, Tucker M G, Wilding M C, Guthrie M and Marrocchelli D 2012 Density-driven structural transformations in network forming glasses: a high-pressure neutron diffraction study of GeO_2 glass up to 17.5 GPa *J. Phys.: Condens. Matter* **24** 415102

[11] Lelong G, Cormier L, Ferlat G, Giordano V, Henderson G S, Shukla A and Calas G 2012 Evidence of fivefold-coordinated Ge atoms in amorphous GeO_2 under pressure using inelastic x-ray scattering *Phys. Rev.* B **85** 134202

[12] Wezka K, Salmon P S, Zeidler A, Whittaker D A J, Drewitt J W E, Klotz S, Fischer H E and Marrocchelli D 2012 Mechanisms of network collapse in GeO_2 glass: high-pressure neutron diffraction with isotope substitution as arbitrator of competing models *J. Phys.: Condens. Matter* **24** 502101

[13] Marrocchelli D, Salanne M and Madden P A 2010 High-pressure behaviour of GeO_2: a simulation study *J. Phys.: Condens. Matter* **22** 152102

[14] Hong X, Shen G, Prakapenka V B, Newville M, Rivers M L and Sutton S R 2007 Intermediate states of GeO_2 glass under pressures up to 35 GPa *Phys. Rev.* B **75** 104201

[15] Brazhkin V V, Lyapin A G and Trachenko K 2011 Atomistic modeling of multiple amorphous–amorphous transitions in SiO_2 and GeO_2 glasses at megabar pressures *Phys. Rev.* B **83** 132103

[16] Meade C, Hemley R J and Mao H K 1992 High-pressure x-ray diffraction of SiO_2 glass *Phys. Rev. Lett.* **69** 1387–90

[17] Haines J, Lager J M, Chateau C and Pereira A S 2000 Structural evolution of rutile-type and $CaCl_2$-type germanium dioxide at high pressure *Phys. Chem. Miner.* **27** 575–82

[18] Ono S, Hirose K, Nishiyama N and Isshiki M 2002 Phase boundary between rutile-type and $CaCl_2$-type germanium dioxide determined by *in situ* x-ray observations *Am. Mineral.* **87** 99–102

[19] Łodziana Z, Parlinski K and Hafner J 2001 *Ab initio* studies of high-pressure transformations in GeO_2 *Phys. Rev.* B **63** 134106

[20] Micoulaut M, Guissani Y and Guillot B 2006 Simulated structural and thermal properties of glassy and liquid germania *Phys. Rev.* E **73** 031504

[21] Murakami M and Bass J D 2010 Spectroscopic evidence for ultrahigh-pressure polymorphism in SiO_2 glass *Phys. Rev. Lett.* **104** 025504

[22] Rehr J J and Albers R C 2000 Theoretical approaches to x-ray absorption fine structure *Rev. Mod. Phys.* **72** 621–54

[23] Ingalls R, Crozier E D, Whitmore J E, Seary A J and Tranquada J M 1980 Extended x-ray absorption fine structure of NaBr and Ge at high pressure *J. Appl. Phys.* **51** 3158–63

[24] Hong X, Newville M, Prakapenka V B, Rivers M L and Sutton S R 2009 High quality x-ray absorption spectroscopy measurements with long energy range at high pressure using diamond anvil cell *Rev. Sci. Instrum.* **80** 073908

[25] Baldini M, Yang W, Aquilanti G, Zhang L, Ding Y, Pascarelli S and Mao W L 2011 High-pressure EXAFS measurements of crystalline Ge using nanocrystalline diamond anvils *Phys. Rev.* B **84** 014111

[26] Ishimatsu N, Matsumoto K, Maruyama H, Kawamura N, Mizumaki M, Sumiya H and Irifune T 2012 Glitch-free x-ray absorption spectrum under high pressure obtained using nano-polycrystalline diamond anvils *J. Synchrotron Radiat.* **19** 768–72

[27] Chen D, Dong J, Zhang X, Quan P, Liang Y, Hu T, Liu J, Wu X, Zhang Q and Li Y 2013 Suppression of Bragg reflection glitches of a single-crystal diamond anvil cell by a polycapillary half-lens in high-pressure XAFS spectroscopy *J. Synchrotron Radiat.* **20** 243–8

[28] Ravel B and Newville M 2005 ATHENA, ARTEMIS, HEPHAESTUS: data analysis for x-ray absorption spectroscopy using IFEFFIT *J. Synchrotron Radiat.* **12** 537–41
[29] Newville M 2001 EXAFS analysis using FEFF and FEFFIT *J. Synchrotron Radiat.* **8** 96–100
[30] Stern E A and Kim K 1981 Thickness effect on the extended-x-ray-absorption-fine-structure amplitude *Phys. Rev.* B **23** 3781–7
[31] Hong X, Shen G, Prakapenka V B, Rivers M L and Sutton S R 2007 Density measurements of noncrystalline materials at high pressure with diamond anvil cell *Rev. Sci. Instrum.* **78** 103905
[32] Jorgensen J D 1978 Compression mechanisms in alpha-quartz structures—SiO_2 and GeO_2 *J. Appl. Phys.* **49** 5473–8
[33] Ono S, Tsuchiya T, Hirose K and Ohishi Y 2003 High-pressure form of pyrite-type germanium dioxide *Phys. Rev.* B **68** 014103
[34] Shiraki K, Tsuchiya T and Ono S 2003 Structural refinements of high-pressure phases in germanium dioxide *Acta Crystallogr.* B **59** 701–8
[35] Ravel B 2001 ATOMS: crystallography for the x-ray absorption spectroscopist *J. Synchrotron Radiat.* **8** 314–6
[36] Houser B, Alberding N, Ingalls R and Crozier E D 1988 High-pressure study of α-quartz GeO_2 using extended x-ray-absorption fine structure *Phys. Rev.* B **37** 6513–6